CHAPTER 3

GROWTH AND CHARACTERIZATION OF THE MoS_xSe_{2-x} SINGLE CRYSTALS

CONTENTS

3.1 Introduction

It has already been seen that transition metal dichalcogenides are considerably important because of their usefulness as lubricating materials, switching devices, electrodes for photoelectrochemical solar cells etc. The method of direct vapour transport described in the earlier chapter has been found to be quite suitable by several workers[1-4] for growing single crystals of layered compounds. It appears from the literature that there has been no previous attempt to grow the single crystals of molybdenum sulphoselenides. Kline et al[5] reported that the transition metal dichalcogenides (TMDC) form a wide range of solid solutions[6,7] with either mixed metal or chalcogenide composition or both and the properties like crystal structure, bandgap, band positions and stability to corrosion, which are of prime interest to photoelectrochemist might be influenced by changing the composition of the layered crystals. It has been observed that the study of mixed system say $MoS_{2x}Se_{2(1-x)}$ can provide good information about two and three dimensional excitons, interlayer effects and dependence of transition oscillator strength on covalency[8]. In present chapter

author reports the growth and characterization as well as microtopographical studies of molybdenum sulphoselenide single crystals.

3.2 Experimental

High quality quartz ampoules were etched, vacuum backed, and 99.999 % pure molybdenum, spectroscopically standardised, 99.999 % pure sulphur powder and 99.99 % pure selenium powders in stoichiometric proportions were placed in an ampoule 25 mm in diameter and 250 mm long. The total charge about 9-10 gm was used in the experiment. Then the ampoule was evacuated and sealed at a pressure of 10^{-5} torr at a constriction 3 mm in diameter.

The powders were thoroughly mixed by vigorous shaking and the mixture was distributed along the length of ampoule. The ampoule was introduced horizontally into the furnace and the temperatures were slowly increased to 800°C in the manner described in earlier chapter. The ampoule was left at this temperature for 72 hours. Then the furnace was shut down and allowed to cool down to room temperature. A free flowing shining dark mixture resulted from the reaction.

3.3 Growth of Single Crystals

The charge thus prepared was well mixed by vigorous shaking of the ampoule. The powder was then distributed along the length of the ampoule and ampoule was kept in the furnace for the growth of crystals as shown in Fig. 3.1. The furnace temperature was increased slowly, as was done for the charge preparation, to the required final temperature for growth.

The exact growth conditions and the procedure adopted for different compositions have been described in Table 3.1. Figure 3.2 shows in general the temperature gradient maintained along the ampoule. After the required period of growth the furnace was shut off and allowed to cool down to room temperature. The ampoule was broken and crystals were found to be grown along the length of the tube.

The crystals obtained are grey-black, in colour and platelike with the c-axis normal to the plane of plates. They grew directly over the distributed charge inside the ampoule. The description of growth product is presented in Table 3.1. Typical crystals of different compositions showing crystalline size are depicted in Fig. 3.3.

Fig. 3.1 Schematic view of the furnace showing the position of ampoule inside the two zone furnace during crystal growth.

Fig. 3.2 Temperature profile of the furnace.

Fig. 3.3 Typical crystals of differing composition in the series MoS_xSe_{2-x}, showing crystalline size

(1) $MoSe_2$ (2) $MoS_{0.5}Se_{1.5}$

(3) MoSSe (4) $MoS_{1.5}Se_{0.5}$

(5) MoS_2

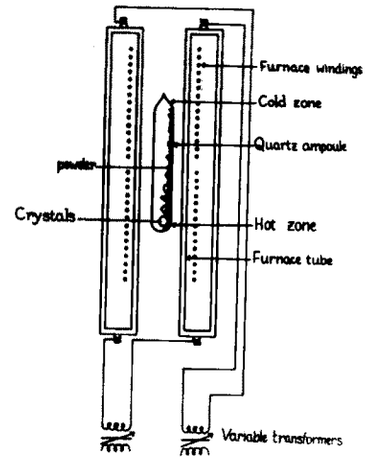

Fig. 3.1

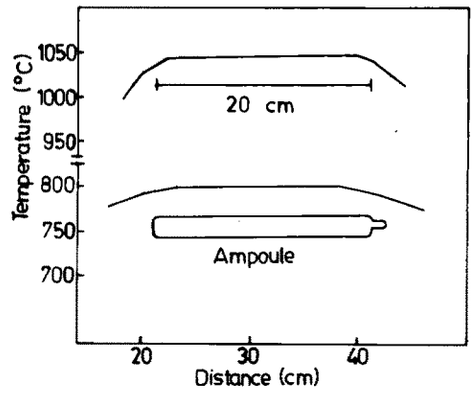

Fig. 3.2

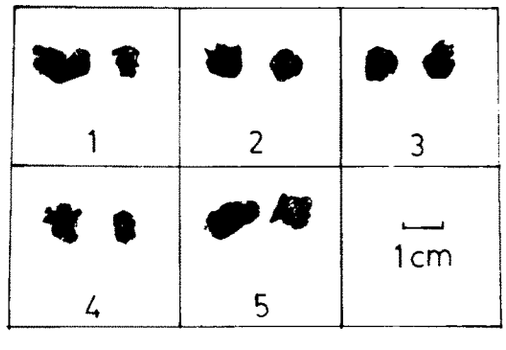

Fig. 3.3

Table 3.1

Growth parameters used to produce single crystals of MoS_xSe_{2-x}

Nominal composition X	Reaction temperature °C	Growth temperature °C	Growth time hours	Crystal size mm x mm x mm	Appearance
0.0	800	1040	168	15 x 10 x 0.3	Gray black
0.5	800	1050	192	13 x 10 x 0.2	Gray black
1.0	800	1060	192	12 x 9 x 0.3	Gray black
1.5	800	1080	216	10 x 10 x 0.2	Gray black
2.0	800	1120	216	15 x 5 x 0.07	Gray black

3.4 Structure

The system MoS_xSe_{2-x} ($0 \leq x \leq 2$) is simple because both the end members $MoSe_2$ and MoS_2 have the same MoS_2 structure (C_7 type). The basic co-ordination unit for the molybdenum in these layered structures is trigonal prismatic. A S-Mo-S sandwich layer is composed of alternately occupied, face-shared prisms, the Mo and S atoms forming close packed layers. No strong bond exists between the layers, only long-range Van der Waal's forces hold atomic sandwiches together. This gives the crystals their characteristic platy habit, with extended growth and pronounced cleavage perpendicular to c-axis. The stacking sequence is AbABaB, where S stacking is represented by capital letters, with the space group D^4_{6h} ($P6_3/mmc$).

3.5 Determination of Lattice Parameters

X-ray diffraction techniques are useful tools for structural investigations. These techniques, based on monochromatic radiation, are important because the d-spacings can be calculated from the observed diffraction angles. In diffractometer, the diffracted radiation is detected by a counter tube which moves through an angular range of reflections. The intensities are recorded on synchronously advancing strip-charts.

The Bragg-Brentano X-ray diffractometer, shown in Fig. 3.4, is used in the present work. Here the specimen is mounted in the center of the diffractometer and rotated by an angle θ around an axis in the specimen plane. The counter is attached to an arm rotating around the same axis by angles twice as large as those of the specimen rotation. Only (hkl) planes parallel to specimen plane contribute to the diffracted intesity.

X-ray diffractometer traces obtained using the diffractometer above, were used to determine the unit cell dimensions are depicted in Figs. 3.5(a) and 3.5(b). The values of lattice parameters 'a' and 'c' determined from the analysis of these traces have been given in Table 3.2. The compositional dependence of lattice parameters and X-ray density are plotted in Fig. 3.6. The 'a' parameter varies linearly with composition according to equation (3.1).

$$a(x) = (3.281 - 0.06315\ x)\ \text{A}^{\circ} \qquad (3.1)$$

where 'x' defines the solid solution MoS_xSe_{2-x}. Variation of the c-parameter is also linear and is given in equation (3.2).

Fig. 3.4 A photograph of X-ray diffractometer HZG 3.

Fig. 3.5(a) X-ray diffractometer traces for $MoSe_2$ and MoS_2 ($CuK\alpha$, λ = 1.5418 Å)

Fig. 3.4

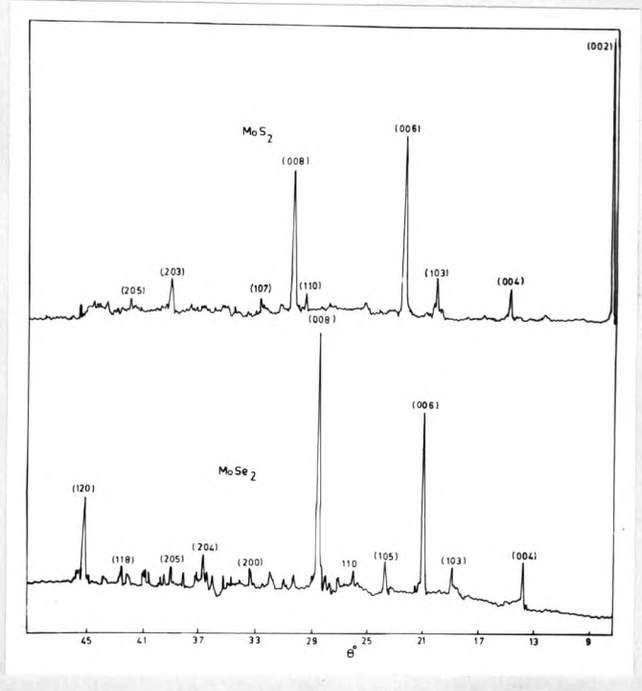

Fig. 3.5(a)

Fig. 3.5(b) X-ray diffractometer traces for $MoS_{0.5}Se_{1.5}$, MoSSe and $MoS_{1.5}Se_{0.5}$ ($CuK\alpha$, λ = 1.5418 Å).

Fig. 3.6 Variation of lattice parameters 'a' and 'c' and X-ray density 'D' with composition 'x' for the series MoS_xSe_{2-x}.

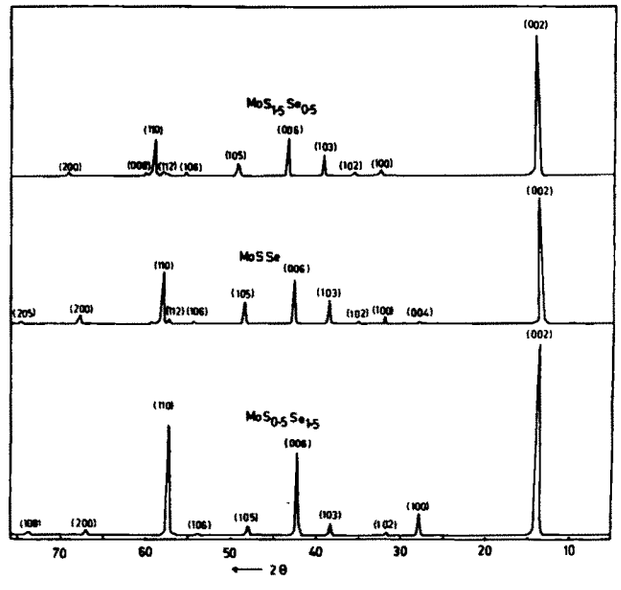

Fig. 3.5(b)

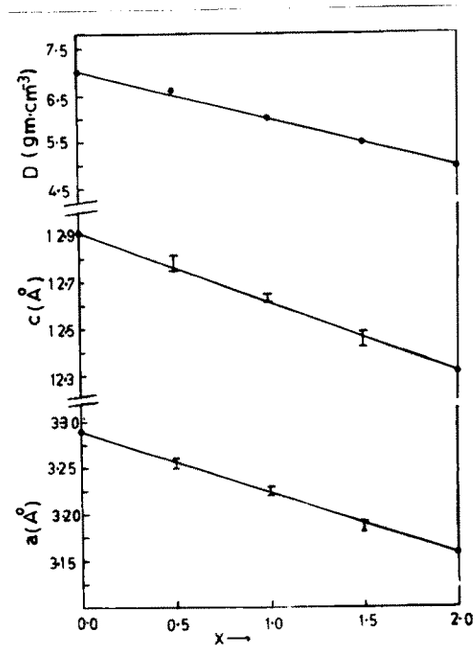

Fig. 3.6

Table 3.2

Structural data and X-ray density, absorption coefficients for series MoS_xSe_{2-x}, $0 \leq x \leq 2$

Nominal composition X	'a' (Å)	'c' (Å)	c/a	X-ray density 'D' gm. cm^{-3}	Absorption coefficient cm^{-1}
0.0	3.283	12.918	3.934	7.000	822.85
0.5	3.254 ± 0.05	12.785 ± 0.03	3.929	6.529	752.96
1.0	3.224 ± 0.01	12.640 ± 0.003	3.920	6.039	726.96
1.5	3.179 ± 0.002	12.463 ± 0.003	3.919	5.583	691.08
2.0	3.166	12.305	3.8866	4.973	656.32

$$c(x) = (12.918 - 0.310\ x)\ \text{A}^{\circ} \qquad (3.2)$$

Densities have been calculated from unit cell dimensions for all compositions. Values of the density, absorption coefficient and c/a ratio are listed in Table 3.2. The density also follows a linear variation (Fig. 3.6) of the form,

$$D(x) = (7.000 - 1.012\ x)\ \text{gm. cm}^{-3} \qquad (3.3)$$

The series of layer compounds form a complete range of isomorphous solid solutions.

3.6 Electron Spectroscopy for Chemical Analysis

For a number of years electron microprobe technique has remained a standard method for microbeam elemental analysis of solid materials. Untill recently, it was also the available technique to investigate the "Surface" composition of a specimen on large scale. During last decade, however a number of new techniques have been developed for the elemental and chemical analysis of solid surfaces and thin films. These techniques involve an excitation of the specimen by X-rays (electron spectroscopy

for chemical analysis, ESCA) by electrons (Auger Electron Spectroscopy, AES) or by ions (Secondary Ion Mass Spectroscopy, SIMS) and the subsequent detection of emitted electrons (ESCA, AES) or ions (SIMS). Compared to electron microprobe, these techniques are extremely surface sensitive and represent a fundamental addition to the analytical capabilities available for the study of composition of materials[9].

The principle of ESCA is as follow, when monoenergetic X-rays impinge upon matter, the electrons are ejected with a kinetic energy E_k, which is determined from the difference between the binding energy of the electron, E_b and the energy of the X-ray photon, $h\nu$. Thus, if the kinetic energy of the ejected electrons is determined, the binding energy of the electron can be evaluated by relationship

$$E_b = h\nu - E_k \qquad (3.4)$$

Since the binding energies of electrons in the outer region of the atomic core depend upon chemical environment, this method can be used to analyze several types of mixtures an analysis of which would be difficult by other means[10].

In practice, the sample is irradiated by monoenergetic X-rays and emitted electrons are analyzed by passage through a double-focusing electron spectrometer.

The ESCA method of analysis is primarily suitable for surface analysis. All elements except hydrogen may be identified, and the oxidation state and bonding of the element is usually determinable. ESCA has been used to study the changes responsible for the poisoning of catalysts, the surface contaminations on semiconductors which may cause poor performance, surface reactions on metals and many other surface phenomena.

Quantitative ESCA measurements have been made on first principle basis. Using Mo, S, Se photoemission peaks areas, calculations are made to evaluate compositions of elements of molybdenum sulphoselenide single crystals, which involve the identification of peaks corresponding to the elements and equating the summation of the ratios of the peak area to the cross-section to 100 %. Figure 3.7 shows the ESCA traces for the energy 0 to 1000 eV. The compositions determined from ESCA are given in Table 3.3.

3.7 Microstructure

A large number of experimental and theoretical

Fig. 3.7 ESCA traces for the composition in the series MoS_xSe_{2-x}, for the energy 0 to 1000 eV.

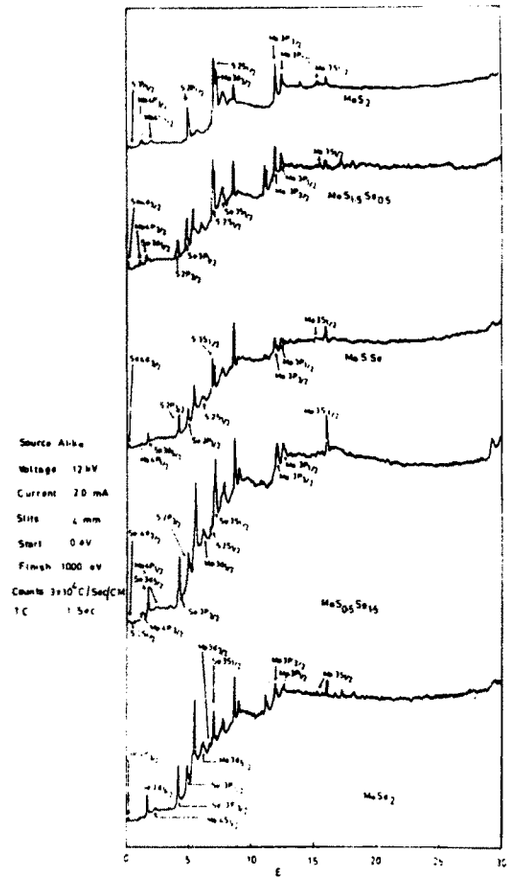
Source Al-ka
Voltage 12 kV
Current 20 mA
Slits 4 mm
Start 0 eV
Finish 1000 eV
Counts 3x10^6 C/Sec(CM
TC 1 Sec
MoS2
MoS1.5Se0.5
MoS Se
MoS0.5Se1.5
MoSe2
0
5
10
15
20
E

Fig. 3.7

Table 3.3

Weight percentage of layer compounds in the series MoS_xSe_{2-x}

obtained by ESCA

Nominal composition x	Observed w %			Calculated w %		
	Mo	S	Se	Mo	S	Se
0.0 ($MoSe_2$)	35.339	-	64.661	37.77	-	62.23
0.5	41.639	6.957	51.404	39.946	7.632	52.422
1.0	49.050	16.472	34.469	46.357	15.491	38.152
1.5	52.306	26.169	21.525	51.259	26.186	22.555
2.0 (MoS_2)	57.487	42.513	-	59.94	40.06	-

Fig. 3.8 Different stages of formation of spiral at a screw dislocation.

Fig. 3.9 Micrograph illustrating growth layers at the edge of crystal.

Fig. 3.10 Micrograph showing the presence of impurities on the crystal surface.

studies[11-19] have been made to understand the crystal growth mechanism. Microtopographical studies of the as-grown faces is one of the methods by which an understanding of the crystal growth and dissolution can be made, mainly because of the fact that habit faces exhibit growth features.

According to Frank's theory[13], thin platelets of basic structures form first by surface nucleation and layer by layer growth takes place under conditions of supersaturation. The crystallites formed at this stage may be perfect or they may contain twins or stacking faults on account of thermodynamic fluctuations during growth. As supersaturation drops below the critical value, the crystal platelets can only thicken further by the addition of material to self-perpetuating steps formed at the site of screw dislocation which may be originated by a buckle-followed-up-slip mechanism as suggested by Frank[13]. As growth proceeds, these steps rotate around the center of the dislocation, finally creating a spiral as shown in Fig. 3.8.

It is well known[11] from the theory of crystal growth that the corners and edges of the crystals can serve as initiation points for the growth layers. An

example showing growth layers at edges is shown in Fig. 3.9. In addition to the edges and corners of the crystals, certain impurities present on the crystal surfaces also serve as nucleation centers for the growth layers. Figure 3.10 reveals such an example of embedded impurities present in crystals.

One of the most striking features of layered crystals is the existence of screw dislocations with Burger's vector perpendicular to the plane of layers giving rise to the growth spirals. Different types of spirals are observed during present studies on microstructures. The surface microstructure on a typical MoSSe single crystal as observed with scanning electron microscope (Philips EM 400) is shown in Fig. 3.11. This photograph reveals the presence of a hexagonal spiral suggesting thereby a screw dislocation mechanism of the growth for these crystals. Sometimes (Fig. 3.12) spirals originate with a circular shape in the beginning and acquire a hexagonal shape in the end. Spirals shown in Fig. 3.13 are having a circular shape and are starting from a common point. Figure 3.14 reveals hexagonal spirals originating from points lying in a straight line and close to each other. It is seen that the spacing between the spirals goes on increasing as they progress outward. Spirals originating from different points show

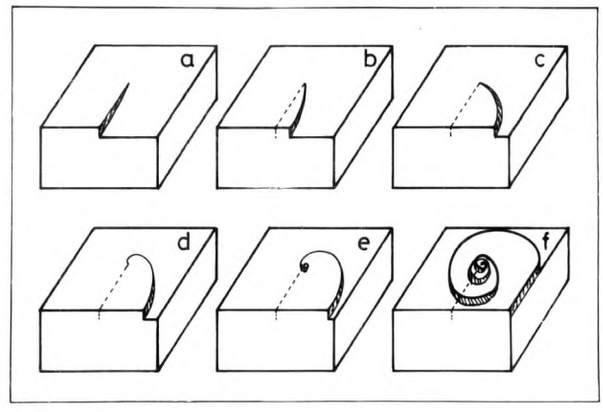

Fig. 3.8

Fig. 3.9 X 90

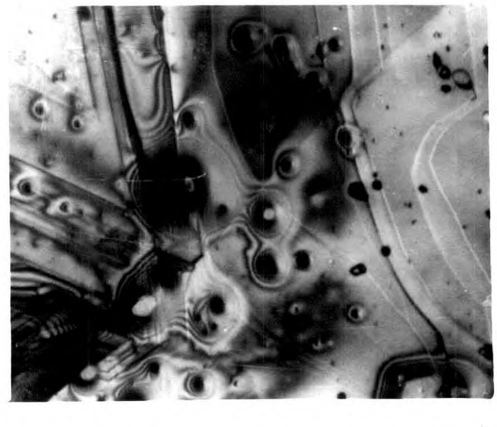

Fig. 3.10 X 90

the distribution of screw dislocations in the as grown crystals. To confirm the fact that emergence point of spirals are the sites of screw dislocations, a MoSSe crystal was etched in 2M H_2CrO_4 for 30 minutes at room temperature. The resulting etch pattern is shown in Fig. 3.15. One can clearly notice the formation of hexagonal etch pits at the emergence points of spirals. The different shapes of the spirals and the variation in spacing between the spiral arms point out that the supersaturation conditions during the growth of the crystals are highly variable.

3.8 Conclusions

1. Single crystals of MoS_xSe_{2-x} have been grown by the direct vapour transport technique, they are observed to be free from contamination by any transporting agent.

2. The crystals are strain-free because they grow vertically in the form of thin platelets directly above the charge.

3. X-ray diffraction studies of the series indicate that all solutions formed are single phase compounds, isomorphous with the

Fig. 3.11 Scanning surface microstructure of MoSSe single crystal using Philips EM 400 Electron Microscope.

Fig. 3.12 A hexagonal spiral having circular shape at center.

Fig. 3.13 Circular spirals of the same sign, originating from common point.

Fig. 3.14 Hexagonal spirals of same sign, starting from different points.

Fig. 3.15 Etch pattern of MoSSe obtained 2 M H_2CrO_4 for 30 min.

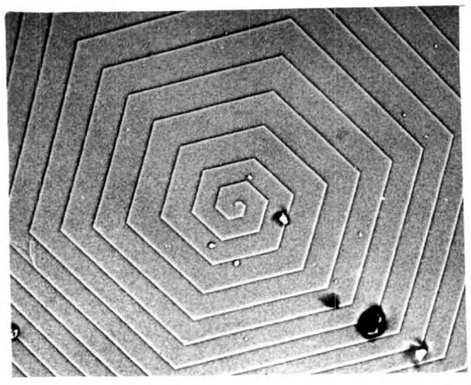

Fig. 3.11 X 200

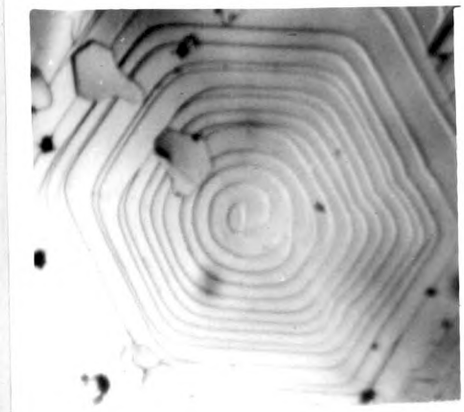

Fig. 3.12 X 95

Fig. 3.13 X 140

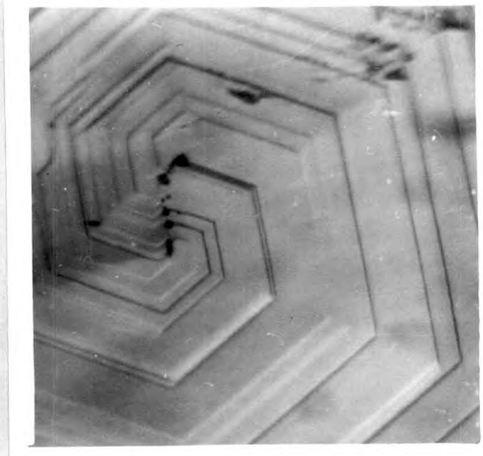

Fig. 3.14 X 235

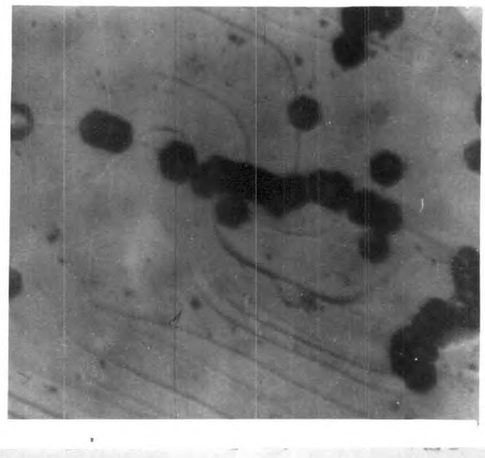

Fig. 3.15 X 140

end members molybdenum diselenide and molybdenum disulphide with MoS_2 type structure.

4. The lattice parameters vary linearly with x.

5. The presence of hexagonal spirals on the faces of the grown crystals suggests a screw dislocation mechanism of growth for these crystals.

References

1. Brixner, L. H. and Teufer, G. (1963)
J. Inorg. Chem. 2, 992.

2. Agarwal, M. K., Patel, H. B. and
Nagi Reddy, K. (1977)
J. Crystal Growth 41, 84.

3. Revolinsky, E. and Beernsten, D. (1964)
J. Appl. Phys. 35, 2086.

4. Al-Hilli, A. A. and Evans, B. L. (1972)
J. Crystal Growth, 15, 93.

5. Kline, G., Kam, K. K., Ziegler, R. and
Parkinson (1982)
Solar Energy Materials, 6, 337.

6. Mentezen, B. F. and Sienko, M. J. (1976)
Inorg. Chem. 15, 2198.

7. Schneemeyer, L. F. and Sienko, M. J. (1980)
Inorg. Chem. 19, 789.

8. Beal, A. R. (1972)
J. Phys. C. 5, 35.

9. Mac Donald, N. C., Riach, C. E. and
Gerlach, R. L. (1976)
Research/Development, 27, 8, 42.

10. Siegbahn, K. (1967)
ESCA : Atomic Molecular and Solid State
Structure Studied by Means of Electron
Spectroscopy.
Alquist and Wiksells. Uppsala.

11. Chase, A. B. (1963)
J. Am. Ceram. Soc. 51, 107.

12. Gruber, E. E. and Mullins, W. W. (1967)
J. Phys. Chem. Solids, 28, 875.

13. Frank, F. C. (1951)
Phil.Mag.. 42, 1014.

14. Cabrera, N. and Levine, M. M. (1956)
Phil. Mag. 1, 450.

15. Burton, W. K., Cabrera, N. and
Frank, F. C. (1951)
Phil. Trans. Roy. Soc. London, A 243, 229.

16. Verma, A. R. (1953)
"Crystal Growth and Dislocations" Butterworths,
London.

17. Sunagawa, I. and Bennama, P. (1981)
J. Crystal Growth, 53, 490.

18. Sunagawa, I., Narita, K., Bennama, P. and Vanderhock, B. (1977)
J. Crystal Growth 42, 121.

19. Mitchel, R. S., Fujiki, Y. and Ishizowa, Y. (1982)
J. Crystal Growth 57, 273.